AFRL-RV-PS-
TR-2013-0110

ASSIMILATIVE MODELING OF OBSERVED POSTMIDNIGHT EQUATORIAL PLASMA DEPLETIONS IN JUNE 2008 (POSTPRINT)

Y.-J. Su, et al.

22 September 2013

Interim Report

AIR FORCE RESEARCH LABORATORY
Space Vehicles Directorate
3550 Aberdeen Ave SE
AIR FORCE MATERIEL COMMAND
KIRTLAND AIR FORCE BASE, NM 87117-5776

DTIC COPY

NOTICE AND SIGNATURE PAGE

Using Government drawings, specifications, or other data included in this document for any purpose other than Government procurement does not in any way obligate the U.S. Government. The fact that the Government formulated or supplied the drawings, specifications, or other data does not license the holder or any other person or corporation; or convey any rights or permission to manufacture, use, or sell any patented invention that may relate to them.

This report was cleared for public release by the 377 ABW Public Affairs Office and is available to the general public, including foreign nationals. Copies may be obtained from the Defense Technical Information Center (DTIC) (http://www.dtic.mil).

AFRL-RV-PS-TR-2013-0110 HAS BEEN REVIEWED AND IS APPROVED FOR PUBLICATION IN ACCORDANCE WITH ASSIGNED DISTRIBUTION STATEMENT.

//SIGNED//	//SIGNED//
Daniel Emmons Program Manager, AFRL/RVBXI	Edward J. Masterson, Colonel, USAF Chief, Battlespace Environment Division

This report is published in the interest of scientific and technical information exchange, and its publication does not constitute the Government's approval or disapproval of its ideas or findings.

REPORT DOCUMENTATION PAGE

Form Approved
OMB No. 0704-0188

1. REPORT DATE *(DD-MM-YYYY)*	**2. REPORT TYPE**	**3. DATES COVERED** *(From - To)*
22-09-2013	Interim Report	12 Feb 2010 – 31 Dec 2012

4. TITLE AND SUBTITLE
Assimilative Modeling of Observed Postmidnight Equatorial Plasma Depletions in June 2008 (Postprint)

5a. CONTRACT NUMBER

5b. GRANT NUMBER

5c. PROGRAM ELEMENT NUMBER
62601F

6. AUTHOR(S)
Y.-J. Su, J. M. Retterer, R. F. Pfaff, P. A. Roddy, O. de La Beaujardiere, and J. O. Ballenthin

5d. PROJECT NUMBER
1010

5e. TASK NUMBER
PPM00005184

5f. WORK UNIT NUMBER
EF004415

7. PERFORMING ORGANIZATION NAME(S) AND ADDRESS(ES)
Air Force Research Laboratory
Space Vehicles Directorate
3550 Aberdeen Avenue SE
Kirtland AFB, NM 87117-5776

8. PERFORMING ORGANIZATION REPORT NUMBER
AFRL-RV-PS-TR-2013-0110

9. SPONSORING / MONITORING AGENCY NAME(S) AND ADDRESS(ES)

10. SPONSOR/MONITOR'S ACRONYM(S)
AFRL/RVBXI

11. SPONSOR/MONITOR'S REPORT NUMBER(S)

12. DISTRIBUTION / AVAILABILITY STATEMENT
Approved for public release; distribution is unlimited. (377ABW-2013-0915 dtd 09 Oct 2013)

13. SUPPLEMENTARY NOTES
JOURNAL OF GEOPHYSICAL RESEARCH, VOL. 116, A09318, doi:10.1029/2011 JA016772, 2011. Government Purpose Rights.

14. ABSTRACT
The Communications/Navigation Outage Forecasting System (C/NOFS) satellite observed large-scale density depletions at postmidnight and early morning local times in the Northern Hemisphere summer during solar minimum conditions. Using electric field data obtained from the vector electric field instrument (VEFI) as input, the assimilative physics-based model (PBMOD) qualitatively reproduced more than 70% of the large-scale density depletions observed by the Planar Langmuir Probe (PLP) onboard C/NOFS. In contrast, the use of a climatological specification of plasma drifts in the model produces no plasma depletions at night. Results from a one-month statistical study found that the large-scale depletion structures most often occur near longitudes of 60°, 140°, and 330°, suggesting that these depletions may be associated with nonmigrating atmospheric tides, although the generation mechanisms of eastward electric fields at postmidnight local times are still uncertain. In this paper, densities obtained from both assimilation and climatology for the entire month of June 2008 are compared with PLP data from C/NOFS and the Challenging Minisatellite Payload (CHAMP), as well as special sensor ionospheric plasma drift/scintillation meter (SSIES) measurements from the Defense Meteorological Satellite Program (DMSP) satellites. Our statistical study has shown that, on average, the densities obtained by the PBMOD, when it assimilates VEFI electric fields, agree better with observed background densities than when PBMOD uses climatological electric fields.

15. SUBJECT TERMS
C/NOFS, equatorial ionospheric modeling

16. SECURITY CLASSIFICATION OF:			**17. LIMITATION OF ABSTRACT**	**18. NUMBER OF PAGES**	**19a. NAME OF RESPONSIBLE PERSON**
a. REPORT	**b. ABSTRACT**	**c. THIS PAGE**			Daniel Emmons
Unclassified	Unclassified	Unclassified	Unlimited	16	**19b. TELEPHONE NUMBER** *(include area code)*

This page is intentionally left blank.

Assimilative modeling of observed postmidnight equatorial plasma depletions in June 2008

Y.-J. Su,[1] J. M. Retterer,[2,3] R. F. Pfaff,[4] P. A. Roddy,[1] O. de La Beaujardière,[1] and J. O. Ballenthin[1]

Received 20 April 2011; revised 12 July 2011; accepted 20 July 2011; published 22 September 2011.

[1] The Communications/Navigation Outage Forecasting System (C/NOFS) satellite observed large-scale density depletions at postmidnight and early morning local times in the Northern Hemisphere summer during solar minimum conditions. Using electric field data obtained from the vector electric field instrument (VEFI) as input, the assimilative physics-based model (PBMOD) qualitatively reproduced more than 70% of the large-scale density depletions observed by the Planar Langmuir Probe (PLP) onboard C/NOFS. In contrast, the use of a climatological specification of plasma drifts in the model produces no plasma depletions at night. Results from a one-month statistical study, we found that the large-scale depletion structures most often occur near longitudes of 60°, 140°, and 330°, suggesting that these depletions may be associated with nonmigrating atmospheric tides, although the generation mechanisms of eastward electric fields at postmidnight local times are still uncertain. In this paper, densities obtained from both assimilation and climatology for the entire month of June 2008 are compared with PLP data from C/NOFS and the Challenging Minisatellite Payload (CHAMP), as well as special sensor ionospheric plasma drift/scintillation meter (SSIES) measurements from the Defense Meteorological Satellite Program (DMSP) satellites. Our statistical study has shown that, on average, the densities obtained by the PBMOD when it assimilates VEFI electric fields agree better with observed background densities than when PBMOD uses climatological electric fields.

Citation: Su, Y.-J., J. M. Retterer, R. F. Pfaff, P. A. Roddy, O. de La Beaujardière, and J. O. Ballenthin (2011), Assimilative modeling of observed postmidnight equatorial plasma depletions in June 2008, *J. Geophys. Res.*, *116*, A09318, doi:10.1029/2011JA016772.

1. Introduction

[2] The Communications/Navigation Outage Forecasting System (C/NOFS) observed many unexpected large-scale plasma density depletions at postmidnight and early morning local times (LTs) during extreme solar minimum conditions [*de La Beaujardière et al.*, 2009; *Burke et al.*, 2009; *Huang et al.*, 2009; *Su et al.*, 2009]. Initial results at the beginning of the C/NOFS mission have been published in a special issue of *Geophysical Research Letters* in 2009. It was shown by *de La Beaujardière et al.* [2009] that such depletions cover about 14° in longitude and 50° in latitude by examining coincident passes of C/NOFS, Challenging Minisatellite Payload (CHAMP), and Defense Meteorological Satellite Program (DMSP) satellites. These depletions were associated with upward plasma drifts and often observed near the America-Africa and India-Indonesia longitude sectors in June and September 2008. *Burke et al.* [2009] studied a 10-day period between 10 and 20 June 2008 and reported that postmidnight equatorial plasma bubbles and deep plasma trenches were intensified after a fast solar wind speed of the corotating interaction region (CIR) encountered the Earth. The following mechanisms have been proposed: (1) The gravitational drift current [*Eccles*, 2004] may acquire sufficient time to build up during extended quiet geomagnetic conditions; (2) the overshielding effect [*Kikuchi et al.*, 2000] may be induced because region 2 currents exceed those of region 1 when the auroral electrojet (AE) index decreases rapidly, particularly after the CIR impinges on the Earth's magnetosphere; and (3) the disturbance dynamo [*Maruyama et al.*, 2005] may take several hours to reach the equator after a geomagnetic disturbance event.

[3] *Huang et al.* [2009] reported that broad plasma density decreases (BPDs) frequently occurred around June Solstices in solar minimum. The widest BPDs were observed in the vicinity of the South Atlantic Anomaly. By examining the neutral density and ion temperature, Huang et al. found that neutral depletions were detected simultaneously with BPDs

[1]Air Force Research Laboratory, Space Vehicles Directorate, Kirtland Air Force Base, New Mexico, USA.
[2]Air Force Research Laboratory, Space Vehicles Directorate, Hanscom Air Force Base, Massachusetts, USA.
[3]Now at Institute for Scientific Research, Boston College, Chestnut Hill, Massachusetts, USA.
[4]NASA Goddard Space Flight Center, Greenbelt, Maryland, USA.

and suggested they were due to a downwelling in the thermosphere and ionosphere.

[4] Using the physics-based model (PBMOD) developed at the Air Force Research Laboratory (AFRL), *Su et al.* [2009] reported simulation results of a depletion event observed on 17 June 2008 by C/NOFS. Two drivers of plasma drifts were exercised: (1) the empirical drift model of *Scherliess and Fejer* [1999] and (2) direct electric field measurements obtained from the vector electric field instrument (VEFI) onboard C/NOFS. Su et al. successfully reproduced density depletions observed at early morning LTs when the PBMOD was driven by electric fields from the VEFI. However, the model produced no depletion at these local times when driven by a climatological drift model. This paper is motivated from our initial result. It is an extended study to cover the entire month of June 2008, when the occurrence frequency of depletion events was highest.

[5] We should note that "trenches," "depletions," and "BPDs" used in previous papers refer to background density reductions distinguishable from the small-scale density fluctuations caused by the equatorial plasma bubbles or spread-*F*, although both signatures are associated with eastward electric fields (i.e., upward plasma drifts) in June 2008. Small-scale fluctuations were often observed imbedded in the large-scale density structure, but large-scale depletions have been frequently observed without small-scale signatures. The primary focus of this paper is a statistical investigation of large-scale density depletions. It is carried out by a model and data comparison. A typical depiction of satellite data is presented in section 2, while the model description and an example of the model output are shown in section 3. In section 4, we report a quantitative comparison between model output and observed density measurements. We also present statistical results from one month of depletion events. Finally, a summary and discussion of this study are contained in section 5.

2. Data Description

[6] In this statistical study, we gather density measurements in June 2008 from seven satellites: C/NOFS, CHAMP, and five DMSP satellites (F13–17). A simple depiction of these satellites and the data availability are described in this section.

2.1. C/NOFS

[7] The C/NOFS mission is a joint effort of the Department of Defense (DoD) Space Test Program led by the Air Force Research Laboratory (AFRL) [*de La Beaujardière et al.*, 2004]. The primary component of the C/NOFS mission is a satellite launched in April 2008 into a low-inclination (13°) elliptical orbit with perigee and apogee altitudes of 400 and 850 km, respectively. The C/NOFS satellite orbits around the equatorial ionosphere through all LTs ~15 times per day (97 min per orbit). Data from two of the five instruments onboard C/NOFS are used in this study: 1-s Planar Langmuir Probe (PLP) ion density data [*Roddy et al.*, 2010] and VEFI electric field measurements [*Pfaff et al.*, 2010]. The latter are converted into plasma drifts to drive the low-latitude ionospheric physics-based model (PBMOD; see section 3), while the former are used to compare with the ionospheric background density output from PBMOD. One-minute average C/NOFS-PLP data are shown in Figure 1a as functions of LT, along with the median density in 0.5 h bins. Without photoionization at night, it is known that the lowest densities occur prior to sunrise, as seen in our data (02:00–05:00 LT in Figure 1a). There are many data points with density below 10^3 cm^{-3}, and the majority of observed density depletion events occurred between midnight and sunrise. These low-density data points do not alter the median values significantly.

2.2. CHAMP

[8] CHAMP is a German satellite launched in July 2000 into a circular, near-polar orbit (inclination = 87°) with an initial altitude of 454 km [*Reigber et al.*, 2002]. Because of atmospheric drag, the satellite altitude decreased over the mission lifetime, and the mission was completed in September 2010. Its LT changed by ~5.5 min d^{-1}, sweeping all time zones in 131 days. The Planar Langmuir Probe (PLP) measured in situ electron densities with a nominal rate of a 1 s sweep every 15 s. Eighteen days (1–18 June) of PLP data are available for June 2008, and the satellite was at an altitude of ~340 km. An inconsistency in the power supply of the instrument caused the large data gap for the remainder of June (private communication with Claudia Stolle). Because our study focuses on low-latitude regions, we select only data within ±13.8° geographic latitude (GLAT). One-minute average CHAMP-PLP data and median density in 0.5 h bins are shown in Figure 1d. The CHAMP data cover only 00:00–03:00 and 12:00–15:00 LT between 1 June and 18 June 2008. The postmidnight densities are 1–2 orders of magnitude lower than those during daytime. Moreover, many measurements were observed with densities of the order of 10^3 cm^{-3}, indicating density depletion events.

2.3. DMSP

[9] DSMP includes a series of satellites in nearly circular, Sun-synchronous orbits (inclination = 98.8°) at a nominal altitude of ~850 km. The plasma densities used in this study were collected from the special sensor ionospheric plasma drift/scintillation meter (SSIES) [e.g., *Heelis and Hanson*, 1998] in June 2008 from five satellites (F13–17). Again, we select data within ±13.8° GLAT. One-minute averaged DMSP-SSIES data are shown in Figure 1d. The ascending equator crossing times of these five satellites are at evening and postsunset LTs (16:00–21:00 LT in Figure 1d), while the descending crossings occur at early morning LTs (04:00–08:00 LT in Figure 1d). The median densities decrease after sunset and increase after sunrise. Again, the lowest densities occur at 04:00–06:00 LT as measured by F14 and F17. In general, the densities observed from DMSP are lower than those from CHAMP, because DMSP satellites are ~400 km higher than the CHAMP satellite.

[10] Our study is focused in the nightside; hence, we display the C/NOFS density data versus geographic longitude (GLON) from 18:00 to 06:00 LT in Figure 1b. Three local minima are identified near 60°, 140°, and 330° GLON. Additionally, many depletion events (density $< 2 \times 10^3$ cm^{-3}) are associated with these local minima. We note that low-density points associated with depletions are much less than 10% of the total number of observations. They do not affect the longitudinal structure of the median values.

[11] In order to understand the evolution of the longitudinal density structure, we plot the median density versus GLON for four different LT sectors, 18:00–21:00 (black),

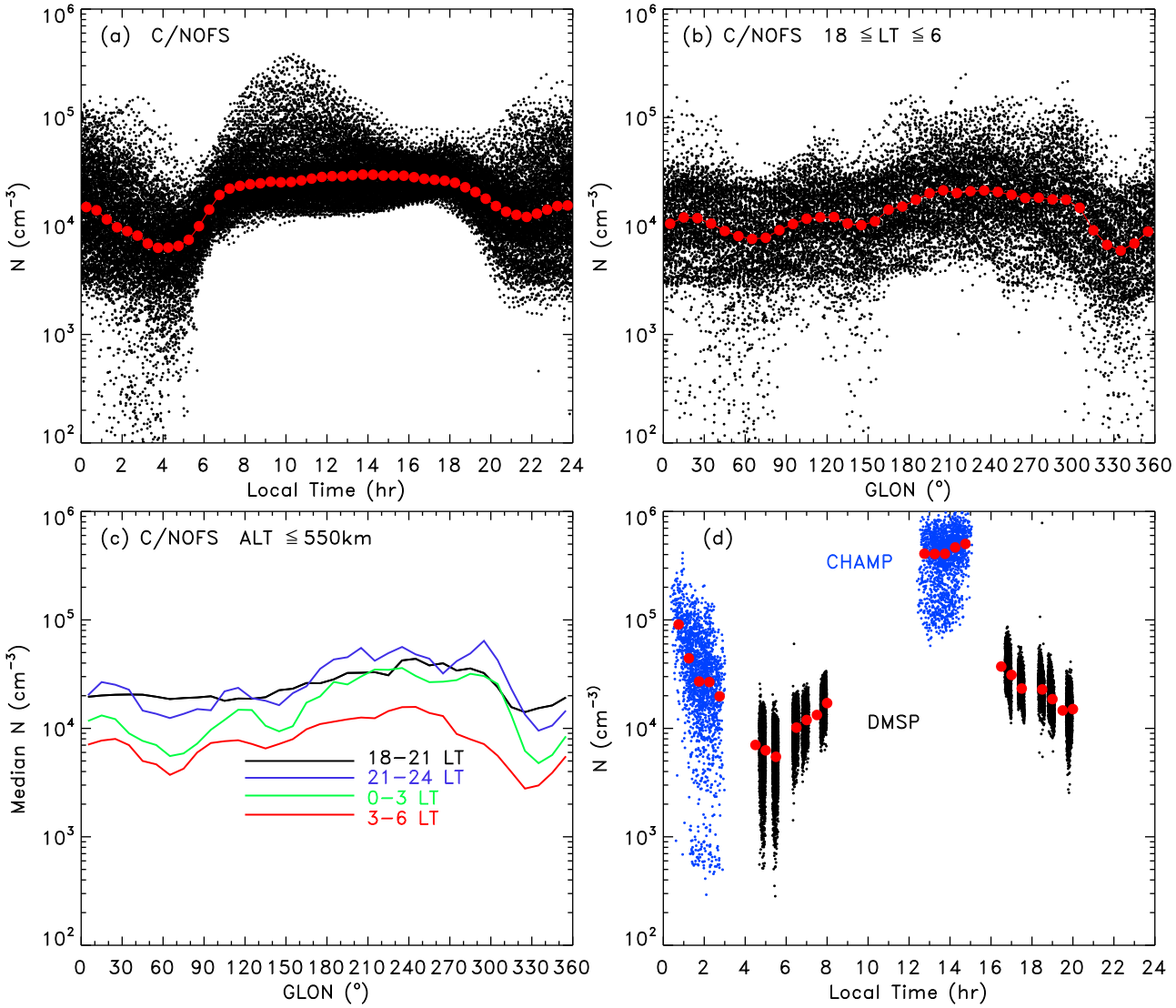

Figure 1. (a) One-minute averaged C/NOFS PLP data (black dots) as functions of LT for all latitudes, longitudes, and altitudes in June 2008. Large red solid circles are used to represent the median density in each 0.5 h bin. (b) One-minute averaged C/NOFS density data (black dots) as functions of GLON at night for all latitudes and altitudes. (c) The median densities as functions of GLON at 18:00–21:00 LT (black line), 21:00–24:00 LT (dark blue line), 00:00–03:00 LT (green line), and 03:00–06:00 LT (red line). (d) One-minute CHAMP (blue dots) and DMSP data (black dots) as functions of LT within ±13.8° GLAT at ~340 and 850 km, respectively.

21:00–24:00 (dark blue), 00:00–03:00 (green), and 03:00–06:00 LT (red) in Figure 1c. We select only C/NOFS data at altitudes less than 550 km in Figure 1c. At 18:00–21:00 LT, one local minimum is identifiable near ~330° GLON. Three local minima appear at 60°, 140°, and 330° GLON from 21:00 to 06:00 LT.

[12] Because of the orbits of the CHAMP and DMSP satellites, ion densities are available only at 00:00–03:00, 04:00–06:00, and 18:00–21:00 LT during the night in June 2008 (see Figure 1d). Density measurements of CHAMP at 00:00–03:00 LT are plotted in Figure 2a. Density observations from C/NOFS at 00:00–03:00 LT between 400 and 450 km are displayed in Figure 2b for comparison. In addition, densities obtained from F13 and F17 at 04:00–06:00 LT are plotted in Figure 2c, while the C/NOFS densities at the same LT sector are displayed in Figure 2d. Because not enough data points are available near the C/NOFS apogee for this statistical study at 04:00–06:00 LT, we include data measured from all altitudes in Figure 2d. Densities obtained from F13, F15, and F16 at 18:00–21:00 LT are shown in Figure 2e. More C/NOFS data points are available at higher altitudes from 18:00 to 21:00 LT, so we restricted the altitude range to between 650 and 850 km in Figure 2f to compare with DMSP observations in Figure 2e.

[13] A longitudinal wave-3 structure is evident in Figure 2. Three local minima appear to be more prominent below 450 km altitude and in the postmidnight sector (Figures 2a and 2b). A fourth minimum can be identified near 270° in

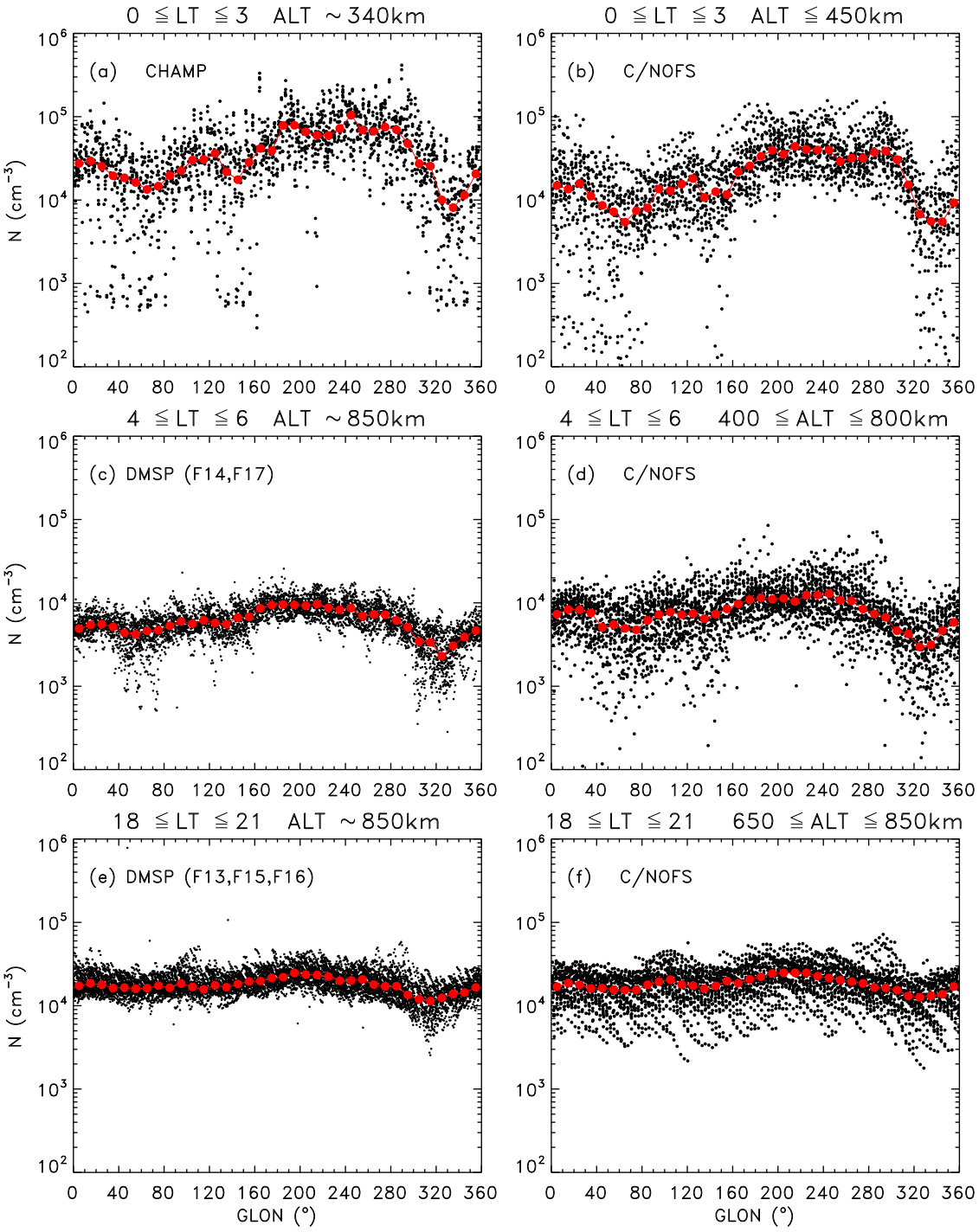

Figure 2. One-minute averaged densities (black dots) as functions of GLON. Large red solid circles represent the median density value in each 0.5 h bin. (a) CHAMP data within 00:00–03:00 LT at ~340 km altitude. (b) C/NOFS data within 00:00–03:00 LT at altitudes between 400 and 450 km. (c) DMSP F13 and F17 data within 04:00–06:00 LT at ~850 km altitude. (d) C/NOFS data within 04:00–06:00 LT for all altitudes (400–800 km). (e) DMSP data from F14, F15, and F17 within 18:00–21:00 LT at ~850 km altitude. (f) C/NOFS data within 18:00–21:00 LT at 650–850 km altitudes.

Figure 2b; however, it is not distinctive at higher altitudes. The median densities of CHAMP are slightly higher than those of C/NOFS because the C/NOFS satellite is located at higher altitudes. Density depletions are associated with three local minima observed from four different satellites (C/NOFS, CHAMP, F14, and F17). In addition, the longitudinal structures at low latitudes, as well as large-scale plasma depletions, are independent of dip latitude (not shown here).

[14] Ion density measurements at night obtained from C/NOFS, CHAMP, and DMSP will be used to compare with the PBMOD density output in section 4.

3. PBMOD

[15] The low-latitude ionospheric physics-based model (PBMOD) has been developed over the last 13 years to support the C/NOFS mission analysis [*Retterer*, 2005]. To set up the initial conditions for the empirical models inputted into PBMOD, a database automatically records parameters such as solar flux, solar wind velocities and densities, interplanetary magnetic fields, and geomagnetic indices. Parameterized by the solar $F_{10.7}$ indices, the *Hinteregger* [1981] reference spectra specify the solar UV fluxes that control photoproduction of plasma and daytime plasma heating. Production and loss rates of O^+ are calculated from the local model originally described by *Jasperse* [1976] and modified throughout the 1980s and 1990s at AFRL. Neutral densities and temperatures are specified by the *Hedin* [1987] Mass Spectrometer Incoherent Scatter (MSIS) model, which is parameterized in terms of the solar $F_{10.7}$ index and the geomagnetic activity index *Ap*. The horizontal neutral wind components are obtained from the most current empirical horizontal wind model (HWM) HWM-07 [*Drob et al.*, 2008; *Emmert et al.*, 2008]. No vertical winds are assumed. The ion and electron temperatures are based on the empirical model published by *Titheridge* [1998] and *Gulyaeva and Titheridge* [2006]. The initial ion densities are given by the FAIM-89 model [*Anderson et al.*, 1989; *Forbes et al.*, 1989]. Zonal drifts are prescribed by the empirical model of *Fejer et al.* [1991] based on Jicamarca observations, while vertical drifts are specified by *Scherliess and Fejer* [1999] based on observations from Jicamarca and the AE-E satellite. Alternatively, the model can be run using $E \times B$ drift velocities obtained from C/NOFS in situ VEFI measurements. Recently, it was shown that when driven by VEFI data, PBMOD successfully reproduced the large-scale postmidnight density depletions on 17 June 2008 [*Su et al.*, 2009]. In this paper, we extend our investigation to cover the entire month of June 2008. For convenience, the term "climatology" represents model runs driven from the empirical drifts, while "assimilation" represents runs driven from VEFI measurements.

[16] The PBMOD solves the continuity equations for both O^+ and H^+ as functions of position and time along the magnetic field lines over a range of apex altitudes in the low-latitude ionosphere. It is based on the LOWLAT model [*Anderson*, 1973] with modifications from *Preble et al.* [1994]. Rather than using a tilted dipole coordinate system, the PBMOD uses magnetic field lines traced from the International Geomagnetic Reference Field (IGRF) model [*International Association of Geomagnetism and Aeronomy Working Group V-MOD*, 2010]. The global model of the PBMOD does not calculate self-consistent fields of plasma perturbations and, therefore, describes only the background ion densities without plasma instabilities. Rayleigh-Taylor instabilities can be simulated by the regional plume model of the PBMOD [*Retterer*, 2010a, 2010b], but it is not relevant for this paper. The global model extends in altitude from 90 to a few thousand kilometers. The model procedure is the same as that used by *Su et al.* [2009] except that H^+ transport equations are run separately from O^+ in this study. The primary reason is that during solar minimum, H^+ ions are often the dominant species at C/NOFS altitudes determined by the ion velocity drift meter (IVM). Using separate H^+ transport equations, we found that results of the PBMOD have reduced dayside densities and increased nightside densities to better agree with observed C/NOFS values. Throughout this paper, simulation results and satellite data are presented in geographic coordinates, although the transport equations are solved and advanced in the field-aligned coordinate system.

[17] Results from 10 June, a geomagnetically quiet day, are presented here as an example (Figure 3). Large-scale plasma depletions were observed frequently throughout the entire day at different longitudinal sectors. The low-latitude ionosphere response to a fast solar wind stream of CIR on 14 June has been published by *Burke et al.* [2009]. In addition, four large-scale depletions modeled by an assimilated PBMOD on 17 June during a fast solar wind stream period can be found in the paper published by *Su et al.* [2009]. Although a local maximum solar wind speed of ~500 km/s was recorded on 8 June by the ACE satellite, the magnitude is 200 km/s less than the CIR event reported by Burke et al. Moreover, the *Kp* index was below 2 throughout 9–10 June. However, the number of depletion events observed by C/NOFS on 10 June is equal to those that occurred after the CIR impinged the Earth's magnetosphere. Thus, large-scale density depletions can occur with or without a strong solar wind driver.

[18] Four structures of large-scale depletions occurred on 10 June (see Figure 3c). The first one began to develop at GLON ~ 50°, ~21:30 UT on 9 June and was observed for three consecutive orbits at 23:15 UT and 0:55 and 2:40 UT on 10 June. (Data from 9 June are not shown here.) The second structure developed at GLON ~ 330°, ~4:00 UT, and lasted two more orbits at 5:50 and 7:25 UT. The magnitude of the second depletion is smaller than that of the first one. The third structure started at GLON ~ 140°, ~17:00 UT, and was observed continuously at 18:45, 20:30 (shown in Figure 3a), and 22:00 UT. Finally, the last depletion developed at GLON ~ 50°, ~23:40 UT, and evolved and disappeared after ~3:00 UT on 11 June. (Data from 11 June are not shown here.) Each of the four structures described here developed after midnight and diminished as the depletions crossed the dawn terminator, similar to the event reported by *Su et al.* [2009]. We are able to reproduce these four structures by assimilative simulations (red line in Figure 3c). Large-scale plasma depletions are associated with upward drifts (positive values in red in Figure 3d). Although the magnitudes of modeled depletions do not precisely match C/NOFS-PLP observations, the occurrence time and geographic location of these structures closely resemble the in situ measurements. In contrast, the model produces no plasma depletions at all when driven by downward velocities at night from a climatological specification of empirical plasma drifts (blue line in Figure 3c).

[19] In order to present the statistical results of our modeling effort, averaged background densities at 450 km altitude in June 2008 are plotted in Figure 4. A wave-three structure can be identified in Figure 4a based on assimilation, where three local maxima (red) are seen near 10°, 100°, and 240° on the dayside and three local minima (blue) are

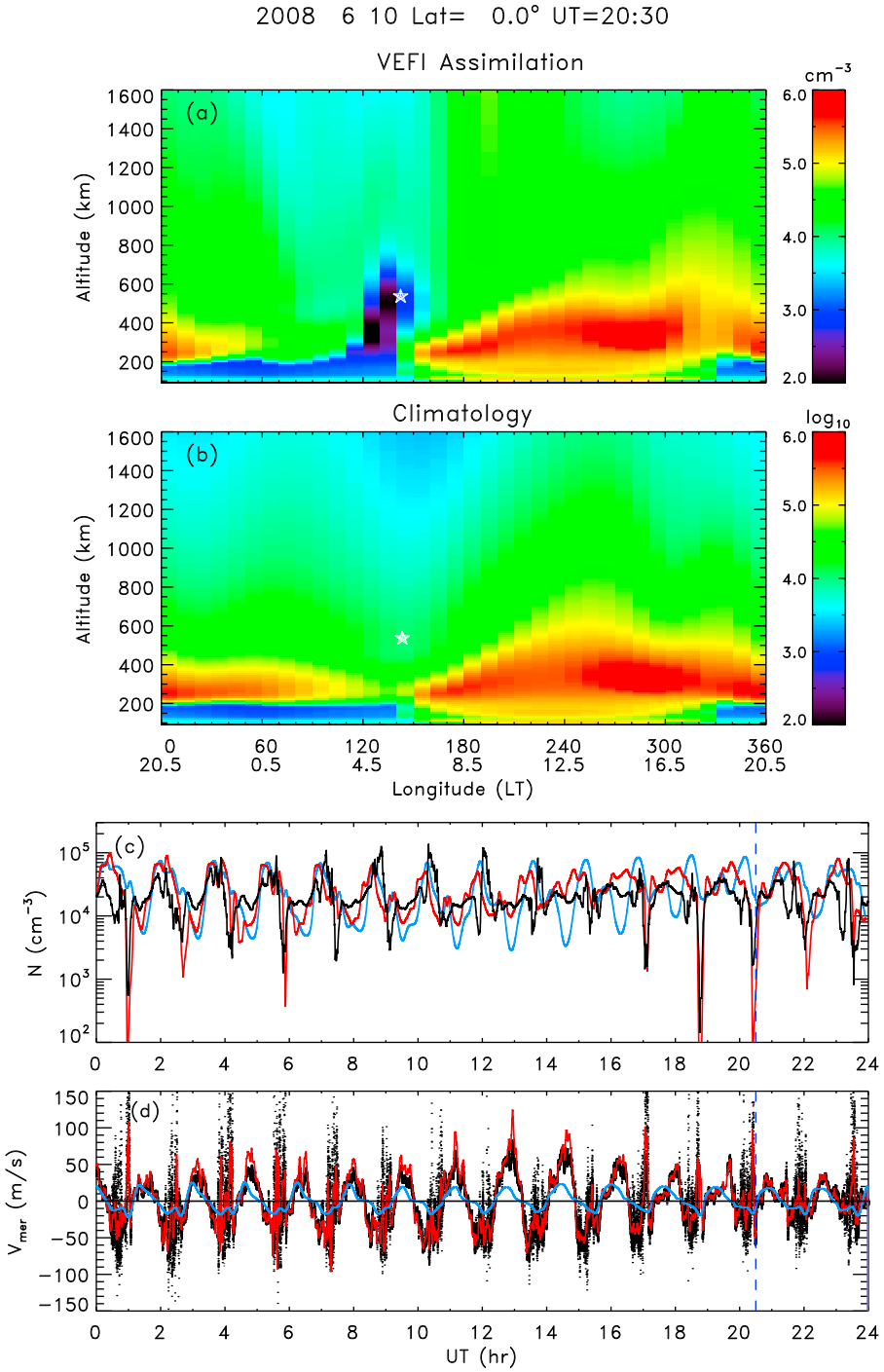

Figure 3. (a) A snapshot of a two-dimensional (2-D) density map obtained from the assimilation model at 0° GLAT, where the *x* and *y* axes represent GLON and altitude, respectively. (b) A 2-D density map based on the climatology model output. The white star denotes the C/NOFS satellite location. Note that the geographic latitude of the satellite at 20:30 UT is 4.9°, not directly in the plane of this 2-D map. (c) Twenty-four hours of C/NOFS PLP smoothed densities on 10 June 2008 are represented by the black line, while the densities along the satellite track from climatology (CLIMO) and assimilation (ASSIM) are shown in blue and red, respectively. (d) Meridional drift velocities with 1 s time resolution obtained from VEFI are represented by small black dots, while the drifts along the satellite track from CLIMO and ASSIM are shown in blue and red lines, respectively. The positive values indicate upward drifts at low magnetic latitudes. A vertical dark blue dashed line in Figures 3c and 3d represent the time (20:30 UT) at which 2-D snapshot images in Figures 3a and 3b were taken.

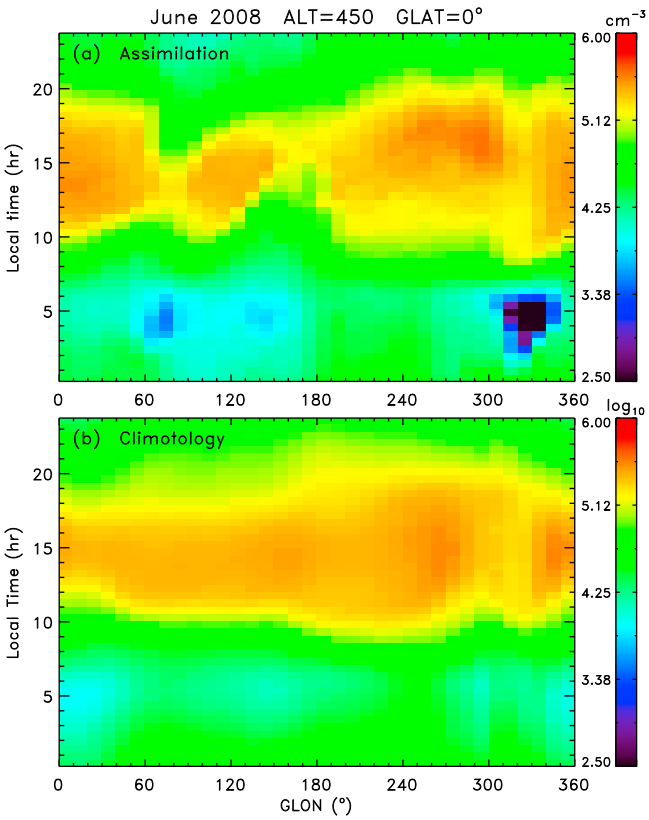

Figure 4. Averaged background ionospheric densities resulting from (a) assimilation and (b) climatology runs at GLAT = 0° and ALT = 450 km for the entire month of June 2008, where the *x* and *y* axes are GLON and LT.

located near 60°, 140°, and 320° at postmidnight. The geographic longitudes of these minima colocate with those shown in Figure 2 based on satellite data.

4. Model-Data Comparison

[20] Quantitative comparisons between model and data densities are presented in this section. Model-to-data density ratios ($N_{PBMOD}/N_{OBSERVE}$) are organized based on each 3 h sector and 10° GLON bin in Figure 5, except that we use 20° GLON bins in Figure 5e because of the fewer number of CHAMP data points. The lines with solid circles represent the median density ratios (i.e., 50th percentile values), and the upper and lower thin lines are the 75th and 25th percentiles, respectively. The width between the upper and lower lines in Figures 5a–5d increases as the night progress because the variations of model-to-data ratios are larger when the background ionospheric densities are lower. In Figures 5a–5e, three or four local maxima are shown by the blue lines (climatology-to-data ratios) near density minima identified in Figures 2 and 4, indicating larger density errors from climatology in these longitudinal sectors. When the median ratio of assimilation (climatology) is closer to the horizontal black line, a red (blue) circle is marked on top of each panel. The numbers of red dots are greater than the numbers of blue dots on top of Figures 5a–5e, indicating that the densities produced from assimilation are closer to the observed values from C/NOFS and CHAMP than those from climatology on average. On the other hand, the climatology works better at the DMSP altitude (Figure 5f). We note that the variations of model-to-data density ratios are smaller on the dayside (not shown) because of the presence of higher background ionospheric densities.

[21] We are interested in the large-scale depletion events that occurred during the deep solar minimum; hence, we intend to determine how well the PBMOD reproduces such events. In order to eliminate small-scale density fluctuations, we utilized the maximum density in each 1 min of PLP data and performed a boxcar average over a 60 s window to represent the background ionospheric density. A large-scale depletion is defined at the location in which the density is observed to have decreased by more than 1order of magnitude within a 5 min window (~20° GLON). The same depletion structure can be observed by C/NOFS over multiple orbits and is counted as a separate case for statistical purposes. The magnitude of the depletion is not taken into account in these statistics. Results are shown in Figure 6a, where 115 cases represented by blue pluses were found based on the C/NOFS-PLP data, while 116 cases represented by black pluses were produced by assimilation of the PBMOD. Large-scale plasma depletions occurred 26% over 446 satellite orbits in June 2008. It should be noted that no such event was generated from the PBMOD climatology. Eighty-three cases (red vertical lines) are identified in which the assimilation reproduced a depletion structure at the same location and time as those observed by C/NOFS. The assimilation tends to underpredict the occurrence of large-scale depletion events between days of year (DOYs) 153 and 159, while it overestimates depletion cases after DOY 173. Between DOYs 160 and 172, ~83% of observed structures have been qualitatively reproduced by the PBMOD assimilation.

[22] We further examine the meridional (vertical) component of drift velocities and find that all depletion cases shown in Figure 6a are associated with upward drifts at the same time or at the same location during the previous orbit. Moreover, the majority of depletion cases occurred postmidnight. Of the 115 C/NOFS cases, 10 were observed between 22:00 and 24:00 LT, and only 1 occurred at postsunset LT. No case was produced prior to 23:00 LT based on the PBMOD assimilation.

[23] A histogram of the depletion occurrence frequency is plotted in Figure 6b, where the blue and red bars represent the depletion cases obtained from C/NOFS and assimilation, respectively. Each vertical bar indicates the counts in each 15° GLON bin. Three local maxima of the occurrence frequency are near 50°, 140°, and 320° GLON. The assimilative PBMOD appears to reproduce the observed depletion structures quite well near 50° and 320° longitude sectors; however, it underestimates events occurring near 140° GLON and overestimates occurrences near 270° GLON.

5. Summary and Discussion

[24] A longitudinal wave-three density structure with local minima near 60°, 140°, and 320° is observed based on the C/NOFS, CHAMP, DMSP data, as well as the PBMOD assimilation, for the entire month of June 2008. The occurrence frequency of large-scale density depletion events is associated with these local minima. Based on the varia-

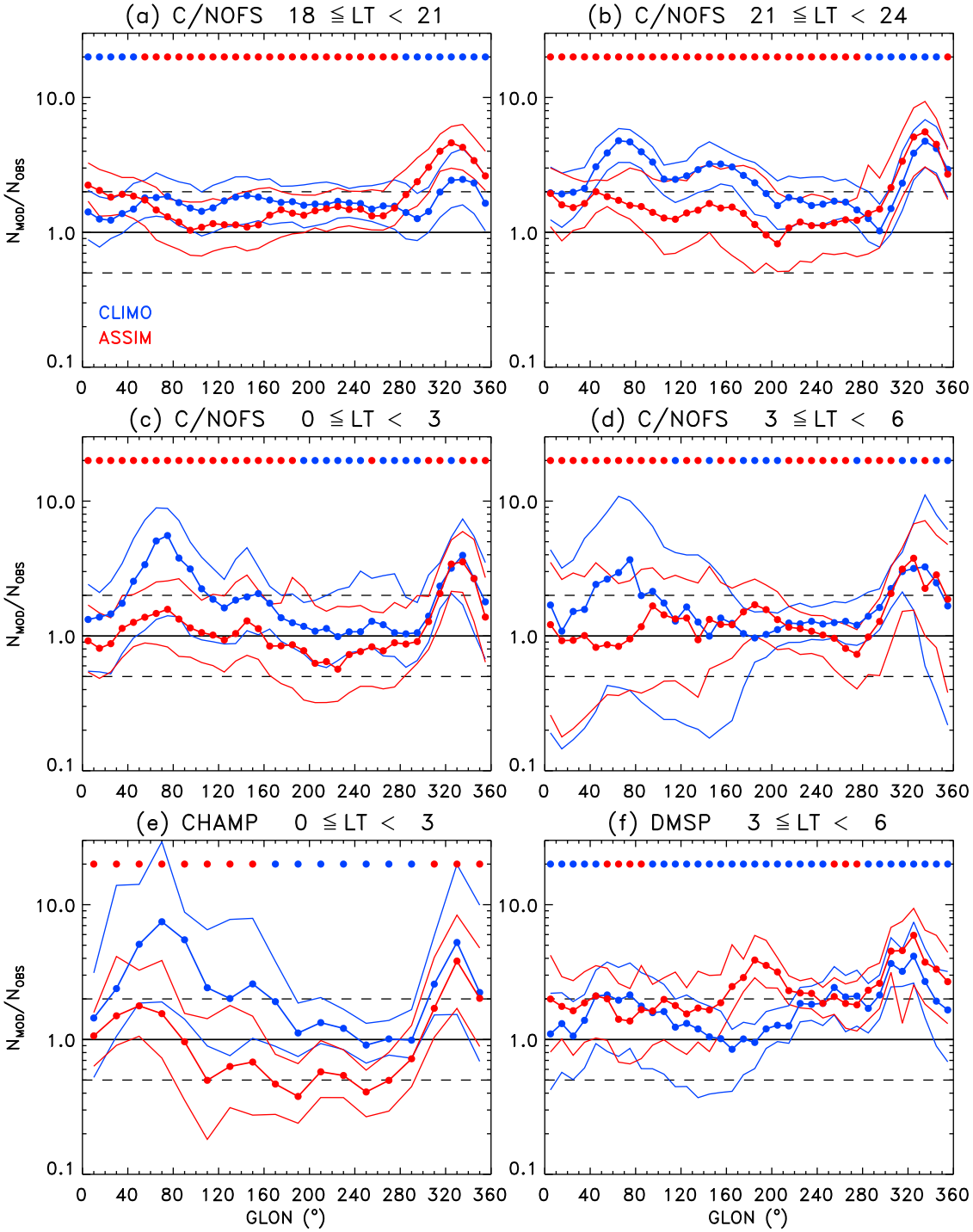

Figure 5. Comparison of density ratios of $N_{\mathrm{PBMOD}}/N_{\mathrm{OBSERVE}}$ between assimilation (red) and climatology (blue) at different local time sectors for different satellites, where the lines with solid circles represent the median density ratios (i.e., 50th percentile) for each 10° longitude bin, and the upper and lower thin lines are the 75th and 25th percentiles, respectively. The range of each longitude bin is 20° in Figure 5e. The bold horizontal black line indicates the perfect model-to-data ratio ($N_{\mathrm{PBMOD}}/N_{\mathrm{OBSERVE}} = 1$), while the upper and lower horizontal dashed lines represent the ratios of 2 and 0.5, respectively. A row of solid circles on top of each part shows the comparison results for each longitudinal bin, where each red circle indicates that the assimilation is better than the climatology, while blue circles represent the opposite.

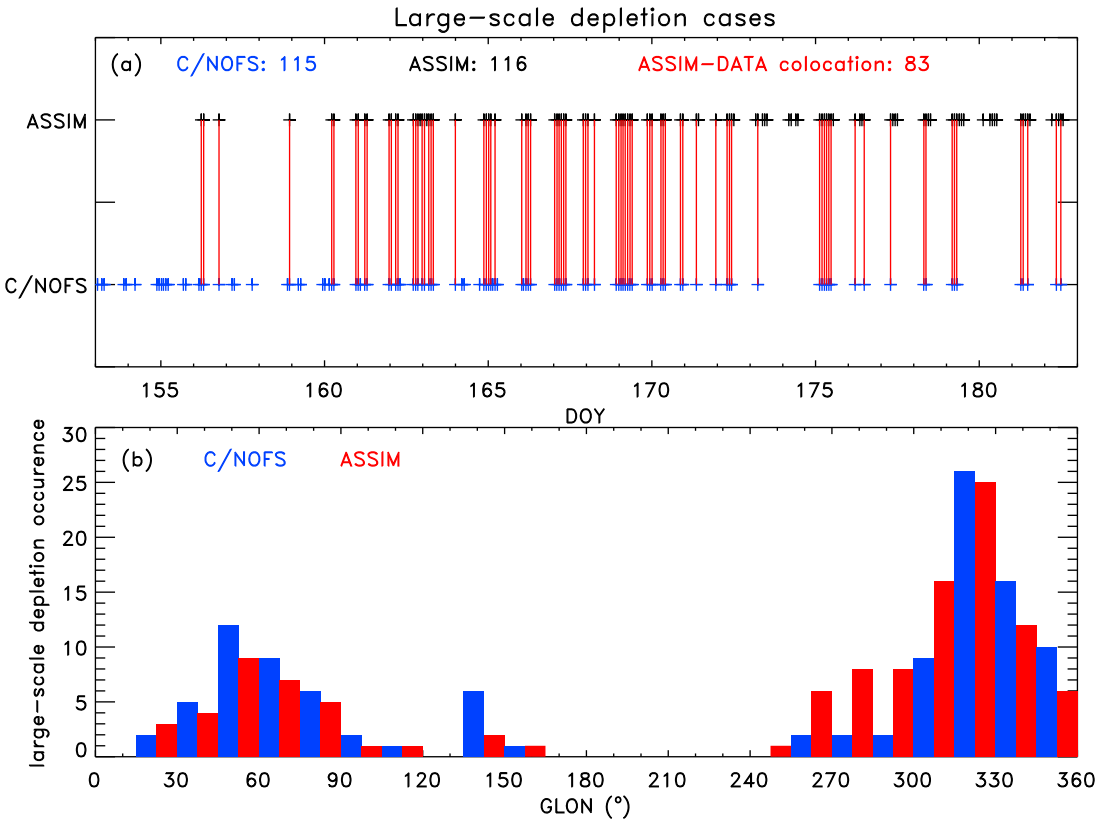

Figure 6. (a) Large-scale depletion cases in June 2008, where the blue and black pluses represent the cases based on the C/NOFS-PLP data and the PBMOD assimilation, respectively. The horizontal red lines indicate where the simulative model reproduced depletions at the same location as those observed from C/NOFS. (b) A histogram of large-scale depletion occurrence versus GLON, where the vertical blue and red bars represent C/NOFS observations and assimilation, respectively.

tions of ion densities obtained from DMSP F17 at 17:30 LT during northern summer months (May–August) in 2007 and 2008, Figure 1d of *Huang et al.* [2010] also indicated three local minima at the same longitudinal sectors as shown in our paper. Huang et al. suggested the DMSP longitudinal density structure is related to lower-atmospheric tides. From $\Delta N/N$ values from C/NOFS during May 2008 through March 2010, *Dao et al.* [2011] recently concluded that the nighttime density irregularities exhibit a longitudinal distribution resembling diurnal meridional winds of tidal waves predicted by the global scale wave model (GSWM). Hence, it is logical to associate the large-scale depletions observed from C/NOFS and CHAMP with atmospheric tides as well.

[25] *Burke et al.* [2009] showed that equatorial ionospheric bubbles and deep plasma trenches were intensified after a fast solar wind stream of CIR reached the Earth on 14 June (DOY 166) because of the overshielding effect where an enhanced high-latitude electric field mapped down to the magnetic equator, producing eastward electric fields. An upward drift velocity (i.e., $E_{\text{east}} \times B_{\text{north}}$) lifted the ionospheric plasma upward, producing large-scale density depletions and/or making the ionosphere unstable to form bubbles (i.e., density irregularities). In this paper, we demonstrate that low-latitude large-scale plasma depletions occurred frequently in summer during extreme solar minimum conditions with or without a strong solar wind driver. The number of depletion occurrences, the 3 h *Kp* indices, and the solar wind velocities from DOYs 153 to 182 are plotted in Figure 7. The cross polar cap potential (i.e., high-latitude electric field) resembles the *Kp* profile; hence, it is not shown here to avoid redundancy. In Figure 7, the geomagnetic indices appear to respond to the increases in solar wind bulk speed; however, the occurrence frequency does not have the same correlation. For example, there are as many depletion events observed on DOY 162 as on DOY 167 (Figure 7, top), while the difference in the solar wind speed is more than 300 km/s (see DOYs 160 and 166 on Figure 7 (bottom)). In addition, the occurrence frequency is high on DOY 175; however, the solar wind speed is below 400 km/s. We do not rule out the contribution of overshielding or disturbance dynamo, but eastward electric fields at postmidnight do exist with or without geomagnetic disturbances, based on the fact that all depletion cases reported here are associated with upward drifts. These eastward electric fields may result from the *E*-region dynamo, where neutral winds are altered by nonmigrating tides [e.g., *Immel et al.*, 2006; *Wan et al.*, 2008; *Liu et al.*, 2010]. Electric field measurements from VEFI represent an extremely complex system. It is currently impossible to separate various effects from a single instrument. Unfortunately, the neutral wind meter (NWM) onboard C/NOFS was not able to accurately determine the neutral wind parameters because of a lack of detectable neutrals during extreme solar minimum conditions. The sensor was designed to be flown during solar

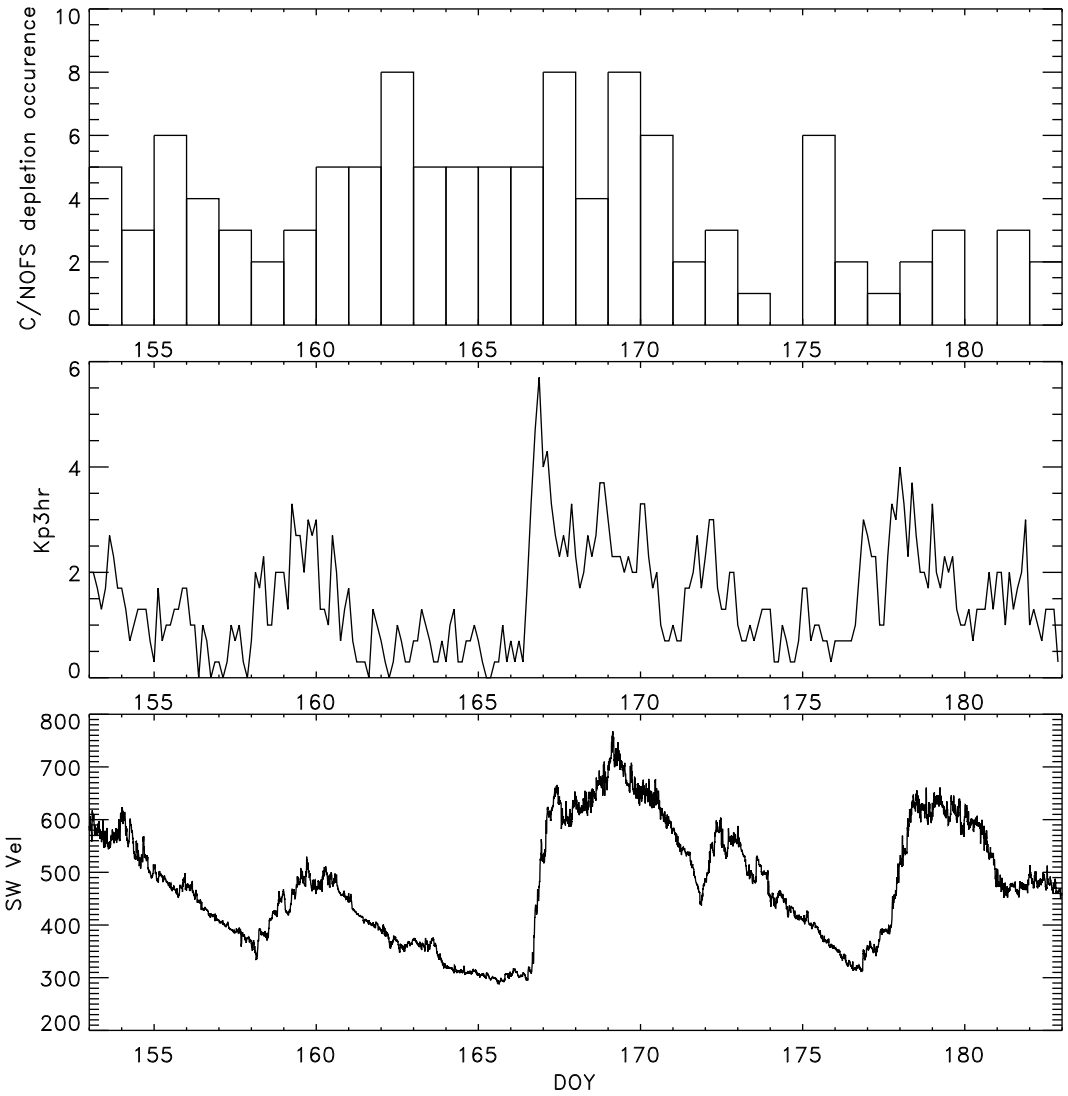

Figure 7. (top) A histogram of the occurrence of large-scale density depletions, (middle) the 3 h *Kp* indices, and (bottom) the solar wind velocities in June 2008.

maximum. Our ability to make progress toward determining the generation of eastward electric fields will be greatly improved with more accurate neutral wind measurements in the future.

[26] Using electric field measurements obtained from VEFI as input, *Su et al.* [2009] were the first to demonstrate that the assimilative PBMOD reproduced a depletion event observed by PLP for four consecutive C/NOFS orbits. In contrast, no plasma depletions were reported when the PBMOD was driven by an empirical drift model. In this paper, we extended our simulations for 30 days in June 2008. The assimilative model reproduces qualitatively more than 70% of the large-scale density depletions observed by PLP onboard C/NOFS. All events were associated with observed upward drifts simultaneously and/or at the same location during the previous orbit. We further confirm that the PBMOD does not produce any depletion at night when driven by a climatological specification of downward plasma drifts. The assimilation underpredicts the occurrence of depletion events during the first 7 days of June, while it overestimates the number of cases during the last 10 days of the month. Between 8 June and 20 June, ~83% of the observed structures have been successfully generated by assimilation, although the magnitude of the depletions may not match precisely those observed from PLP.

[27] Finally, the model-to-data density ratios have been examined in detail for quantitative comparisons between outputs from assimilation, climatology, and satellite data, including C/NOFS, CHAMP, and DMSP. Because of the nature of this comparison, the variations in the ratio are larger when the background density is lower; however, the median assimilation-to-data density ratios at night are within the range between 0.3 and 10. Our statistical study has shown that, on average, the densities obtained by the PBMOD when it assimilates VEFI electric fields agree better with observed densities than those obtained using climatology electric fields. This holds for all local times at night, particularly at lower altitudes such as CHAMP and C/NOFS locations. In general, the use of climatological electric fields results in greater overestimation of density than the use of assimilated

electric fields, except when comparing with DMSP data at 850 km altitude.

[28] The prediction of background ionospheric densities has been qualitatively and quantitatively shown to improve by ingesting VEFI data along the satellite orbit. Accurate measurements of plasma drifts and/or electric fields certainly increase the accuracy of forecasted plasma densities in the low-latitude ionosphere.

[29] **Acknowledgments.** The C/NOFS mission is supported by the Air Force Research Laboratory, the Department of Defense Space Test Program, NASA, the Naval Research Laboratory, and The Aerospace Corporation. The first author thanks Gordon Wilson for providing DMSP data, Louise Gentile for useful conversation regarding CIR events, Han-Li Liu at NCAR for providing references on nonmigrating tides, and Ron Caton for proofreading the manuscript. We also thank the referees for their positive comments and helpful questions. This research task was supported in part by the NASA grant NNH09AK051 to AFRL.

[30] Robert Lysak thanks the reviewers for their assistance in evaluating this paper.

References

Anderson, D. N. (1973), A theoretical study of the ionospheric *F*-region equatorial anomaly, I. theory, *Planet. Space Sci.*, *21*, 409–419, doi:10.1016/0032-0633(73)90040-8.

Anderson, D. N., J. M. Forbes, and M. Codrescu (1989), A fully analytical, low- and middle-latitude ionospheric model, *J. Geophys. Res.*, *94*, 1520–1524, doi:10.1029/JA094iA02p01520.

Burke, W. J., O. de La Beaujardière, L. C. Gentile, D. Hunton, R. F. Pfaff, P. A. Roddy, Y.-J. Su, and G. R. Wilson (2009), Plasma density and electric field irregularities observed by C/NOFS at post-midnight local times, *Geophys. Res. Lett.*, *36*, L00C09, doi:10.1029/2009GL038879.

Dao, E., M. C. Kelley, P. Roddy, J. Retterer, O. de La Beaujardière, and Y.-J. Su (2011), Longitudinal and seasonal dependence of nighttime equatorial plasma density irregularities during solar minimum detected on the C/NOFS satellite, *Geophys. Res. Lett.*, *38*, L10104, doi:10.1029/2011GL047046.

de La Beaujardière, O., et al. (2004), C/NOFS: A mission to forecast scintillations, *J. Atmos. Sol. Terr. Phys.*, *66*, 1573–1571, doi:10.1016/j.jastp.2004.07.030.

de La Beaujardière, O., et al. (2009), C/NOFS observations of deep plasma depletions at dawn, *Geophys. Res. Lett.*, *36*, L00C06, doi:10.1029/2009GL038884.

Drob, D. P., et al. (2008), An empirical model of the Earth's horizontal wind fields: HWM07, *J. Geophys. Res.*, *113*, A12304, doi:10.1029/2008JA013668.

Eccles, J. V. (2004), The effect of gravity and pressure in the electrodynamics of the low-latitude ionosphere, *J. Geophys. Res.*, *109*, A05304, doi:10.1029/2003JA010023.

Emmert, J. T., D. P. Drob, G. G. Shepherd, G. Hernandez, M. J. Jarvis, J. W. Meriwether, R. J. Niciejewski, D. P. Sipler, and C. A. Tepley (2008), DWM07 global empirical model of upper thermospheric storm-induced disturbance winds, *J. Geophys. Res.*, *113*, A11319, doi:10.1029/2008JA013541.

Fejer, B., E. de Paula, S. González, and R. Woodman (1991), Average vertical and zonal F region plasma drifts over Jicamarca, *J. Geophys. Res.*, *96*, 13,901–13,906, doi:10.1029/91JA01171.

Forbes, J. M., D. N. Anderson, M. Codrescu, and P. P. Batista (1989), An analytical/empirical model of the middle and low latitude ionosphere, *Rep. GL-TR-89-0096*, Air Force Geophys. Lab., Hanscom AFB, Mass.

Gulyaeva, T. L., and J. E. Titheridge (2006), Advanced specification of electron density and temperature in the IRI ionosphere-plasmasphere model, *Adv. Space Res.*, *38*(11), 2587–2595, doi:10.1016/j.asr.2005.08.045.

Hedin, A. E. (1987), MSIS-86 thermospheric model, *J. Geophys. Res.*, *92*, 4649–4662, doi:10.1029/JA092iA05p04649.

Heelis, R. A., and W. B. Hanson (1998), Measurements of thermal ion drift velocity and temperature using planar sensors, in *Measurement Techniques in Space Plasmas: Particles*, *Geophys. Monogr. Ser.*, vol. 102, edited by R. F. Pfaff, J. E. Borovsky, and D. T. Young, pp. 61–71, AGU, Washington, D. C.

Hinteregger, H. (1981), Observational, reference, and model data on solar EUV from measurements on AE-E, *Geophys. Res. Lett.*, *8*, 1147–1150, doi:10.1029/GL008i011p01147.

Huang, C.-S., F. J. Rich, O. de La Beaujardiere, and R. A. Heelis (2010), Longitudinal and seasonal variations of the equatorial ionospheric ion density and eastward drift velocity in the dusk sector, *J. Geophys. Res.*, *115*, A02305, doi:10.1029/2009JA014503.

Huang, C. Y., F. A. Marcos, P. A. Roddy, M. R. Hairston, W. R. Coley, C. Roth, S. Bruinsma, and D. Hunton (2009), Broad plasma decreases in the equatorial ionosphere, *Geophys. Res. Lett.*, *36*, L00C04, doi:10.1029/2009GL039423.

Immel, T. J., E. Sagawa, S. L. England, S. B. Henderson, M. E. Hagan, S. B. Mende, H. U. Frey, C. M. Swenson, and L. J. Paxton (2006), Control of equatorial ionospheric morphology by atmospheric tides, *Geophys. Res. Lett.*, *33*, L15108, doi:10.1029/2006GL026161.

International Association of Geomagnetism and Aeronomy Working Group V-MOD (2010), International Geomagnetic Reference Field: The eleventh generation, *Geophys. J. Int.*, *183*(3), 1216–1230, doi:10.1111/j.1365-246X.2010.04804.x.

Jasperse, J. R. (1976), Boltzmann-Fokker-Planck model for the electron distribution function in the Earths ionosphere, *Planet. Space Sci.*, *24*, 33–40, doi:10.1016/0032-0633(76)90058-1.

Kikuchi, T., H. Liihr, K. Schlegel, H. Tachihara, M. Shinohara, and T.-I. Kitamura (2000), Penetration of auroral electric fields to the equator during a substorm, *J. Geophys. Res.*, *105*, 23,251–23,261, doi:10.1029/2000JA900016.

Liu, H.-L., W. Wang, A. D. Richmond, and R. G. Roble (2010), Ionospheric variability due to planetary waves and tides for solar minimum conditions, *J. Geophys. Res.*, *115*, A00G01, doi:10.1029/2009JA015188.

Maruyama, N., A. D. Richmond, T. J. Fuller-Rowell, M. V. Codrescu, S. Sazykin, F. R. Toffoletto, R. W. Spiro, and G. H. Millward (2005), Interaction between direct penetration and disturbance dynamo electric fields in the storm-time equatorial ionosphere, *Geophys. Res. Lett.*, *32*, L17105, doi:10.1029/2005GL023763.

Pfaff, R., et al. (2010), Observations of DC electric fields in the low latitude ionosphere and their variations with local time, longitude, and plasma density during extreme solar minimum, *J. Geophys. Res.*, *115*, A12324, doi:10.1029/2010JA016023.

Preble, A. J., D. N. Anderson, B. G. Fejer, and P. H. Doherty (1994), Comparison between calculated and observed F region electron density profiles at Jicamarca, Peru, *Radio Sci.*, *29*, 857–866, doi:10.1029/94RS00825.

Reigber, C., H. Luhr, and P. Schwintzer (2002), CHAMP mission status, *Adv. Space Res.*, *30*(2), 129–134, doi:10.1016/S0273-1177(02)00276-4.

Retterer, J. M. (2005), Physics-based forecasts of equatorial radio scintillation for the Communication and Navigation Outage Forecasting System (C/NOFS), *Space Weather*, *3*, S12C03, doi:10.1029/2005SW000146.

Retterer, J. M. (2010a), Forecasting low-latitude radio scintillation with 3-D ionospheric plume models: 1. Plume model, *J. Geophys. Res.*, *115*, A03306, doi:10.1029/2008JA013839.

Retterer, J. M. (2010b), Forecasting low-latitude radio scintillation with 3-D ionospheric plume models: 2. Scintillation calculation, *J. Geophys. Res.*, *115*, A03307, doi:10.1029/2008JA013840.

Roddy, P. A., D. E. Hunton, J. O. Ballenthin, and K. M. Groves (2010), Correlation of in situ measurements of plasma irregularities with ground-based scintillation observations, *J. Geophys. Res.*, *115*, A06303, doi:10.1029/2010JA015288.

Scherliess, L., and B. G. Fejer (1999), Radar and satellite global equatorial F region vertical drift model, *J. Geophys. Res.*, *104*, 6829–6842, doi:10.1029/1999JA900025.

Su, Y.-J., J. M. Retterer, O. de La Beaujardière, W. J. Burke, P. A. Roddy, R. F. Pfaff Jr., G. R. Wilson, and D. E. Hunton (2009), Assimilative modeling of equatorial plasma depletions observed by C/NOFS, *Geophys. Res. Lett.*, *36*, L00C02, doi:10.1029/2009GL038946.

Titheridge, J. (1998), Temperatures in the upper ionosphere and plasmasphere, *J. Geophys. Res.*, *103*, 2261–2277, doi:10.1029/97JA03031.

Wan, W., L. Liu, X. Pi, M.-L. Zhang, B. Ning, J. Xiong, and F. Ding (2008), Wavenumber-4 patterns of the total electron content over the low latitude ionosphere, *Geophys. Res. Lett.*, *35*, L12104, doi:10.1029/2008GL033755.

J. O. Ballenthin, O. de La Beaujardière, P. A. Roddy, and Y.-J. Su, AFRL/RVBXP, BEL Bldg 570, 3671 Aberdeen Ave, S.E., Kirtland AFB, NM 87117, USA. (Yi-Jiun.Su@kirtland.af.mil)

R. F. Pfaff, NASA Goddard Space Flight Center, Code 696, Greenbelt, MD 20771, USA.

J. M. Retterer, Institute for Scientific Research, Boston College, 400 St. Clement's Hall, 140 Commonwealth Ave., Chestnut Hill, MA 02467-3862, USA.

DISTRIBUTION LIST

DTIC/OCP
8725 John J. Kingman Rd, Suite 0944
Ft Belvoir, VA 22060-6218 1 cy

AFRL/RVIL
Kirtland AFB, NM 87117-5776 2 cys

Official Record Copy
AFRL/RVBXI/Jack W. Hines 1 cy